Earth and Planetary Science Letters
December 2011, Volume 312, Issues 3–4, Pages 443–452
http://dx.doi.org/10.1016/j.epsl.2011.10.008

Evidence for intense REE scavenging at cold seeps from the Niger Delta margin

G. Bayon[a, *], D. Birot[a], L. Ruffine[a], J.-C. Caprais[b], E. Ponzevera[a], C. Bollinger[c, d], J.-P. Donval[a], J.-L. Charlou[a], M. Voisset[a], S. Grimaud[e]

[a] Ifremer, Département Géosciences Marines, F-29280 Plouzané, France
[b] Ifremer, Département Etude des Ecosystèmes Profonds, F-29280 Plouzané, France
[c] Université Européenne de Bretagne, F-35000 Rennes, France
[d] Université de Brest, IUEM, CNRS UMS 3113, F-29280 Plouzané, France
[e] TOTAL, CSTJF Av. Larribau, F-64019 Pau Cedex, France

*: Corresponding author : G. Bayon, Tel.: + 33 2 98 22 46 30 ; fax: + 33 2 98 22 45 70 ;
email address : gbayon@ifremer.fr

Abstract:

For many trace elements, continental margins are the location of intense exchange processes between sediment and seawater, which control their distribution in the water column, but have yet to be fully understood. In this study, we have investigated the impact of fluid seepage at cold seeps on the marine cycle of neodymium. We determined dissolved and total dissolvable (TD) concentrations for REE and well-established tracers of fluid seepage (CH_4, TDFe, TDMn), and Nd isotopic compositions in seawater samples collected above cold seeps and a reference site (i.e. away from any fluid venting area) from the Niger Delta margin. We also analyzed cold seep authigenic phases and various core-top sediment fractions (pore water, detrital component, easily leachable phases, uncleaned foraminifera) recovered near the hydrocast stations.

Methane, TDFe and TDMn concentrations clearly indicate active fluid venting at the studied seeps, with plumes rising up to about 100 m above the seafloor. Depth profiles show pronounced REE enrichments in the non-filtered samples (*TD* concentrations) within plumes, whereas filtered samples (*dissolved* concentrations) exhibit slight REE depletion in plumes relative to the overlying water column and display typical seawater REE patterns. These results suggest that the net flux of REE emitted into seawater at cold seeps is controlled by the presence of particulate phases, most probably Fe–Mn oxyhydroxides associated to resuspended sediments. At the reference site, however, our data reveal significant enrichment for dissolved REE in bottom waters, that clearly relates to diffusive benthic fluxes from surface sediments.

Neodymium isotopic ratios measured in the water column range from ε_{Nd} ~−15.7 to − 10.4. Evidence that the ε_{Nd} values for Antarctic Intermediate waters (AAIW) differed from those reported for the same water mass at open ocean settings shows that sediment/water interactions take place in the Gulf of Guinea. At each site, however, the bottom water ε_{Nd} signature generally differs from that for cold seep minerals, easily leachable sediment phases, and detrital fractions from local sediments, ruling out the possibility that seepage of methane-rich fluids and sediment dissolution act as a substantial source of

dissolved Nd to seawater in the Gulf of Guinea. Taken together, our data hence suggest that co-precipitation of Fe–Mn oxyhydroxide phases in sub-surface sediments leads to quantitative scavenging of dissolved REE at cold seeps, preventing their emission into bottom waters. Most probably, it is likely that diffusion from suboxic surface sediments dominates the exchange processes affecting the marine Nd cycle at the Niger Delta margin.

Highlights

► Fluid seepage at margins does not represent a source of dissolved REE to the ocean. ► FeMn oxide precipitation at cold seeps leads to quantitative removal of dissolved REE. ► Diffusive fluxes from suboxic sediments probably play a major role in marine Nd cycle.

Keywords : rare earth elements; neodymium isotopes; seawater; cold seeps; Fe–Mn oxyhydroxides; benthic fluxes

1 – Introduction

1.1. The sources of dissolved neodymium to the ocean

The distribution of neodymium isotope ratios in seawater matches remarkably well global ocean circulation patterns (see Frank, 2002; Goldstein and Hemming, 2003 for summaries). On this basis, neodymium isotopes have been increasingly used as water-mass tracers in marine authigenic precipitates and biogenic sediments to improve understanding of past ocean circulation (e.g., Rutberg et al., 2000; Piotrowski et al., 2005, 2009; Scher and Martin, 2004; Pucéat et al., 2005; van de Flierdt et al., 2006; Haley et al., 2008; Gutjahr et al., 2008; Robinson and van de Flierdt, 2009). Despite significant interest in using Nd isotopes for paleoceanographic studies, the way water masses acquire their Nd isotopic composition is not fully understood yet. In fact, the sources of dissolved Nd and other rare earth elements (REE) to the ocean are still being debated. Hydrothermal systems probably do not contribute much to the dissolved Nd oceanic budget, because Nd and other rare earth elements emitted at vent sites are efficiently scavenged by iron-rich plumes (e.g., Michard et al., 1983; German et al., 1990; Halliday et al., 1992; Sherrel et al., 1999). To a first approximation, therefore, dissolved neodymium in seawater is derived from continental inputs, with possible contributions from rivers (e.g., Goldstein and Jacobsen, 1987; Elderfield et al., 1990; Sholkovitz, 1995; Sholkovitz et al., 1999; Sholkovitz and Szymczak, 2000), dissolution of settling particles (e.g., German and Elderfield, 1990; Greaves et al., 1994; Tachikawa et al., 1999; Nozaki and Alibo, 2002; Bayon et al., 2004; Jacobson and Holmden, 2006), submarine groundwater discharge (Johannesson and Burdige, 2007), and benthic fluxes (e.g., Elderfield and Sholkovitz, 1987; Sholkovitz et al., 1992; Amakawa et al., 2000; Lacan and Jeandel, 2005; Arsouze et al., 2007, 2009). The Nd isotopic composition in ocean basins hence globally reflects the age of surrounding terranes.

63 A major advance in the understanding of the marine Nd cycle has been the recognition over
64 recent years that the Nd isotopic signature of water masses could be modified along
65 continental and island margins, without any significant additional input of dissolved Nd
66 (Jeandel et al., 1998; Tachikawa et al., 1999; Lacan and Jeandel, 2001; Lacan and Jeandel,
67 2004a; Lacan and Jeandel, 2004b; Lacan and Jeandel, 2005; Andersson et al., 2008;
68 Amakawa et al., 2009). Lacan and Jeandel (2005) referred to this process as 'boundary
69 exchange', suggesting that ocean margins were an important component of the oceanic Nd
70 cycle. Recent modeling studies even proposed that exchange processes at margins could
71 represent the dominant source of dissolved Nd to the ocean (up to ~90%), far more important
72 than inputs from rivers and aeolian particles taken together (Arzouse et al., 2007; Arzouse et
73 al., 2009). However, despite the evidence that sediment/water interactions at margins play a
74 key role in the marine Nd geochemistry, the mechanisms of this exchange are not well
75 understood. Dedicated studies are now needed to better constrain the processes behind
76 boundary exchange. There are few sources of dissolved REE at margins that could possibly
77 impact the oceanic Nd budget at a global scale, which include dissolution of lithogenic
78 sediments, benthic fluxes from sub-surface sediments, and venting of methane-rich fluids
79 from reducing sediments. The goal of the present work is to assess, for the first time, the
80 potential importance of this latter source (i.e. fluid seepage) in the marine Nd cycle.
81
82 **1.2. Cold seeps and emission of methane-rich fluids on margins**
83 Venting of methane-rich fluids is a widespread phenomenon at ocean margins. Although
84 there are large uncertainties in estimating the mass of methane stored in marine sediment
85 (Judd et al., 2002), it is likely that methanogenesis occurs over at least 30% of the world's
86 continental margins (Hovland and Judd, 1992). Seafloor expressions of focused fluid venting
87 are commonly referred to as cold seeps, which include a large range of geological structures

such as pockmarks, mud volcanoes, gas chimneys, and brine pools. In marine sediment, methane is typically produced through microbial degradation of organic matter under anoxic conditions, after a specific sequence of reactions, which greatly affect pore water chemistry (e.g. Froelich et al., 1979; Thomson et al., 1993). In particular, organic matter degradation in reducing sediments can lead to significant enrichments (from 10 to 1,000 times) in the rare earth element contents of pore waters relative to seawater (Elderfield and Sholkovitz, 1987; Haley et al., 2004).

Because methane, as a greenhouse gas, plays a key role in the Earth's climate, there have been significant efforts to quantify methane fluxes at continental margins, and assess their relevance to the global carbon budget (e.g., Judd et al., 2002; Milkov et al., 2003; Kopf, 2003; Wallmann et al., 2006). In marked contrast, however, very little is known about trace element biogeochemistry at cold seeps, and the impact of fluid seepage on ocean chemistry. A few dedicated studies have focused on the geochemical cycling of barium at cold seeps from the Peru and California margins (Torres et al., 1996; 2002; Castellini et al., 2006; McQuay et al., 2008). These studies showed that emission of dissolved Ba at vent sites had significant local impact on the marine Ba budget. Similarly, fluid seepage on continental margins could also represent a potential source of dissolved Nd to the ocean, but to the best of our knowledge, there has been no comparable work for the rare earth elements.

Here, we report dissolved and total dissolvable (TD) REE concentrations, Nd isotopic compositions, and data for well-established tracers of fluid seepage (CH_4, TDFe, TDMn) for seawater samples collected in the water column above deep-sea fluid-escape structures from the Niger Delta (Gulf of Guinea, West African margin). In addition, we also present data for a series of pore water samples, sub-surface sediments and associated authigenic precipitates

113 from the same area. Our data demonstrate that fluid seepage at cold seeps is not accompanied
114 by emission of dissolved REE into bottom waters, because Fe-oxyhydroxide co-precipitation
115 leads to quantitative REE scavenging at vent sites.
116
117 **2 – Regional setting**
118 **2.1. Studied sites**
119 The area investigated in this study is located on the Niger Delta, between 500 m and 1800 m
120 water depth (Fig. 1). A large number of seafloor structures related to fluid venting (i.e., mud
121 volcanoes, diapirs, pockmarks) were reported previously on the Niger Delta deep province
122 (Mascle et al., 1973; Brooks et al., 1994; Cohen and McClay, 1996; Bayon et al., 2007; Sultan
123 et al., 2010). In this study, all water and sediment samples were collected from three distinct
124 areas (Fig. 1). 1) A pockmark-rich area (water depth: ~ 550m; hereafter referred to as
125 Pockmark Field), characterized by the presence of large seafloor depressions with irregular
126 shapes (Fig. 2a). 2) A mud volcano (~ 680 m water depth; about 1km wide) situated on the
127 north flank of a dome, composed of two distinct volcanic cones with a mean elevation of
128 about 40m (Fig. 2b). The dome also exhibits a wide range of fluid venting structures related
129 to the presence of faults and/or gas hydrate reservoirs. 3) An area located at ~ 1780 m water
130 depth (Reference Site), where several submarine slope failures were reported previously
131 (Sultan et al., 2007), but which is not characterized by any active fluid seepage. In addition, a
132 few pore water samples were collected from sub-surface sediments recovered from other
133 active pockmarks of this Niger Delta area (see Bayon et al., 2007).
134
135 **2.2. Hydrography of the Gulf of Guinea**
136 The surface layer of the eastern tropical Atlantic is composed of warm and poorly salted
137 Tropical Surface Water (TSW; Fig. 3). The low salinity of TSW is largely attributable to

intense river runoff and rainfall in the Gulf of Guinea (Fig. 3A). At about 70 m depth, the base of TSW is marked by a broad salinity maximum in the temperature range 17- 22 °C (Fig. 3B), which corresponds to Subtropical Underwater (STUW). Below STUW, the South Atlantic Central Water masses (SACW) extend up to ~500 m depth, characterized by a nearly linear temperature - salinity relationships (Fig. 3B). The water mass below SACW corresponds to colder (~5°C) and fresher (salinity ~34.5) Antarctic Intermediate Water (AAIW), centered at about 800 m depth. Finally, the deeper water masses in the study area are dominated by southward-flowing North Atlantic Deep Water (NADW). Circulation patterns of the upper water masses are quite complex in the Niger Delta area (Fig. 1). Surface waters are transported eastward by the Guinea Current (GC), while circulation of water masses below 100 m is dominated by the westward-flowing Northern South Equatorial Current (nSEC).

3 – Sampling and methods

Samples were collected during previous expeditions to the Niger Delta aboard N/O *Atalante* (NERIS project, 2004) and N/O *Pourquoi Pas?* (ERIG-3D project, 2008). All seawater samples were collected during the ERIG-3D cruise using 8 l PVC-bottles mounted on a CTD-rosette assembly. For determination of methane concentrations, aliquots of 125 ml were collected in glass bulbs on board, and stored in a cold room to await transportation to the laboratory in Brest. Then, methane was analysed using a chromatographic purge/trap technique (Charlou and Donval, 1993; Charlou et al., 1998). For total dissolvable trace element analyses (TDFe, TDMn, TDREE), a 60 ml aliquot of non filtered seawater was transferred into acid-cleaned polyethylene bottles, and acidified to ~ pH 2 with ultra-pure twice sub-boiled HNO_3. For dissolved REE studies, 250 ml seawater samples were filtered through 0.45µm cellulose filters. After filtration, seawater samples were acidified to ~ pH 2

163 with ultra-pure twice sub-boiled HNO_3, prior to addition of Tm spike. The REE were then
164 extracted from the filtered samples by ferric-hydroxide co-precipitation, after addition of NH_4
165 (Bayon et al., 2011). For Nd isotope measurements, between ~ 5 and 20 l of seawater were
166 filtered and acidified to ~ pH 2. At Brest, Nd and other REE were then pre-concentrated by
167 ferric-hydroxide co-precipitation, followed by purification using cation exchange (AG 50W-
168 X8) and Ln-resin columns.
169
170 A series of sub-surface sediment samples recovered by either piston or gravity coring near the
171 hydrocast stations were also analysed in this study (see core location in Fig. 2). Pore waters
172 were extracted from bulk sediments on board by centrifugation and filtered (0.45 µm)
173 immediately. Upon availability, ~ 3 to 40 ml aliquots of pore waters were processed for
174 determination of REE concentrations, following the procedure described above (Bayon et al.,
175 2011). Uncleaned foraminifera fractions (mainly *Globigerinoides ruber*) were analysed to
176 gain additional information on the ε_{Nd} signature of bottom waters, as demonstrated recently
177 by Roberts et al. (2010). Foraminifera fractions were cleaned in ultrasonic bath with ultra
178 pure water, prior to dissolution using dilute HNO_3 acid. The terrigenous fraction of every
179 studied sediment sample was also analysed after removal of carbonate and Fe-oxyhydroxide
180 phases from the bulk sediment (Bayon et al., 2002). In addition, the fine-grained (< 45 µm)
181 fraction of each core-top sediment sample was leached (room T°C, 24 h) using ultra-pure
182 dilute (0.05% v/v) nitric solution (i.e. easily leachable fraction), in order to assess the
183 potential contribution of sediment dissolution to the non-filtered seawater samples. The acid
184 strenght of this dilute nitric solution exactly matches that of the solution (pH ~ 2) in which
185 non-filtered seawater samples were stored prior to analysis. Then, dilute HNO_3 leachates
186 were filtered (0.45 µm) before processing for REE and Nd isotope measurements. Finally,
187 two methane-derived carbonate concretions and authigenic gypsum were hand-picked from

188 the Pockmark Field and Mud Volcano sediments, cleaned using ultra pure water, and
189 analysed to provide direct information on the pore water ε_{Nd} signature at the studied cold seep
190 sites.
191
192 All measurements were made at the Pôle Spectrométrie Océan (PSO), Brest. Rare earth
193 element, Fe and Mn concentrations were measured with an ELEMENT 2 ICP-SFMS. The
194 REE were analysed with the low resolution mode to enhance sensitivity, but were corrected
195 for interferences following the procedure of Bayon et al. (2009). Rare earth element
196 concentrations were calculated using the Tm addition method (Barrat et al., 1996; Bayon et
197 al., 2009). Details on the applicability of this method for determining REE abundances in
198 seawater are given elsewhere (Bayon et al., 2011; Freslon et al., 2011). For Fe and Mn, the
199 ELEMENT2 was operated in medium resolution mode. Procedural blanks for Fe and Mn
200 corresponded to ~ 1.5 nM and ~ 0.5 nM, respectively. Neodymium isotopic ratios were
201 determined by Neptune MC-ICP-MS. Analysis of the JNdi-1 standard during the analytical
202 session gave $^{143}Nd/^{144}Nd$ of 0.512115 ± 0.000011 (2 s.d., n=12), which corresponds in epislon
203 notation (DePaolo and Wasserburg, 1976) to an ε_{Nd} value of = -10.16 ± 0.21. Total
204 procedural blanks were less than 1 ng for Nd, which represented less than 6% of the mass of
205 Nd in the measured fraction of seawater samples.
206
207 **4 – Results and Discussion**
208
209 **4.1. Depth profiles at the active venting sites: Pockmark Field and Mud Volcano sites**
210 The bottom water samples at the Pockmark Field (CTD-08) and Mud Volcano (CTD-06)
211 stations exhibit CH_4 values with concentrations up to ~ 2000 nl/l and ~ 330 nl/l respectively,
212 much higher than background seawater values (in the range ~ 15 and 40 nl/l), which clearly

indicate active fluid venting (Table 1). At these two sites, methane plumes rise up to about 100 m above the seafloor (Fig. 4). Iron and manganese oxyhydroxide precipitation typically occurs above methane seeps at submarine hydrothermal systems (e.g. German et al., 1990), but also on continental margins (Charlou et al., 2004), when Fe-rich vent fluids mixed with high pH (pH ~ 8) and oxygen-rich bottom waters. Similarly, here, the plumes at Pockmark Field and Mud Volcano also exhibit distinctive anomalies for both TDMn (up to 8 nmol/L; Table 1) and TDFe (up to ~ 50 nmol/L), which could hence reflect the presence of Fe-Mn oxyhydroxyde particulates. Alternatively, the occurence of Fe and Mn anomalies in non-filtered seawater samples could also indicate partial dissolution of suspended particles entrained within the plumes. High levels of TDREE concentrations were also determined in the methane plumes at both sites (Table 1), with depth profiles for TDNd closely resembling those for TDFe (Fig. 4). Interestingly, while TDNd concentrations are significantly enriched in the methane plumes (up to 62 pmol/kg), the dissolved Nd contents for the same samples are much lower (around 22 pmol/kg; Table 2, Fig. 5), and do not exhibit any significant enrichment relative to the overlying water column (Fig. 5). Overall, these results suggest that venting of methane-rich fluids at cold seeps does not lead to significant emission of dissolved REE into the water column. Our data show however that fluid venting is accompanied by a flux of REE associated with iron-rich particulate phases, which could indicate either co-precipitation of Fe-Mn oxyhydroxides in bottom waters or re-suspension of local sediments.

4.2. Evidence for benthic fluxes at the Reference Site

At the Reference Site, the bottommost water sample (CTD03-B1) exhibits higher TDFe and TDMn concentrations (i.e. the highest TDMn value measured during the course of this study; 10.3 nmol/kg, Table 1) than the overlying water column (Fig. 4). In contrast with the Pockmark Field and Mud Volcano sites, however, these anomalies are most probably due to

238 diffusion from surface sediments at this location, rather than to active fluid venting.
239 Similarly, the same bottommost sample also displays the highest dissolved REE
240 concentrations determined in this study (e.g. [Nd] ~ 27.9 pmol/kg, Table 1). Taken together,
241 these results could suggest that benthic fluxes at the Reference Site (i.e. away from any active
242 fluid venting area) lead to diffusive emission of REE into bottom waters. Evidence that both
243 TDNd and dissolved Nd exhibit similar concentrations at this site, as shown in Fig. 5,
244 indicates however the absence of any significant Fe-oxyhydroxide co-precipitation or
245 sediment resuspension at this station.

246

247 **4.3. Deciphering REE provenance in the filtered and non-filtered seawater samples**

248 To gain further constraints on the origin of REE sources in the methane plumes, we
249 considered shale-normalised REE patterns for both non-filtered (TD data) and filtered
250 (dissolved concentrations) samples (Fig. 6), and compared them to data for pore waters (Table
251 3) and easily leachable sediment fractions (Table 4). For clarity, only REE patterns for
252 selected seawater samples from the Pockmark Field and the Reference Site are shown in Fig.
253 6, but note that similar conclusions could be also drawn using samples from the Mud
254 Volcano.

255

256 At the Pockmark Field, filtered samples collected from within the plume (sample CTD08-B1
257 to –B8; Table 2) all display very similar seawater-like REE patterns (Fig. 6A), characterized
258 by a pronounced negative Ce-anomaly and progressively increasing shale-normalized values
259 from the light- (LREE) to the heavy-REE (HREE). These patterns are very similar to those
260 determined for the seawater samples at the Reference hydrocast station (Fig. 6B). In marked
261 contrast, non-filtered samples collected at the same water depths at the Pockmark Field show

a larger range of REE patterns, with variable Ce-anomalies and various mid-REE (MREE) over LREE enrichments (Fig. 6A). In comparison, pore waters from sub-surface sediments at the Mud Volcano and other active venting sites of the Niger Delta area exhibit REE concentrations about one order of magnitude higher than those for seawater samples (Table 3). These pore water samples display shale-normalized patterns characterized by a positive Ce-anomaly and a MREE enrichment relative to LREE and HREE (Fig. 6A). This MREE-bulge type pattern is a typical feature of anoxic pore waters in marine sediments, interpreted as the consequence of the reduction of sedimentary Fe-oxyhydroxide phases during early diagenesis (Haley et al., 2004). Although we did not analyse any pore water sample from the Pockmark Field area, the carbonate concretion collected from core ER-CS-38 also displays a similar REE pattern (Table 4, pattern not shown here), which suggests that it was formed from fluids having similar REE signature (Rongemaille et al., 2011). Here, the evidence that filtered samples collected from within the methane plume exhibit seawater-like REE patterns that are well distinct from those for local sub-surface pore waters provides strong support that active venting at these seeps does not represent any substantial source of dissolved REE to bottom waters.

As discussed earlier, one explanation accounting for the TDFe, TDMn and TDREE anomalies at both the Pockmark Field and Mud Volcano was that they were due to co-precipitation of Fe-Mn oxyhydroxide phases in bottom waters above venting sites. If this was the case, however, one would expect the filtered samples collected from the methane plumes to have inherited, at least partly, the distinctive REE signature of pore waters. Instead, it is more likely that these anomalies indicate partial dissolution of resuspended particles entrained within the methane plumes. This hypothesis can be demonstrated using simple mass balance calculations with REE concentrations for typical bottom water (e.g., filtered sample CTD08-

B3) and the easily leachable fractions of core-top sediments (Table 4). Comparatively, the REE concentrations determined in the dilute nitric leachates are much higher (i.e., about a factor 10^8) than seawater values. The leaching experiments with dilute HNO_3 led to the extraction of about 20 wt% of the initial mass of sediment. This implies that the presence of even a very small amount of suspended particles in any of our non-filtered seawater samples could have a significant impact on its REE composition. In Fig. 6C, we show that the REE patterns for non-filtered samples from within the plume at the Pockmark Field can be generated by partial dissolution of sediments in seawater samples having total suspended matter loadings (TSM) of about 0.1 to 0.2 mg/l. For comparison, this range of values is similar to the maxima TSM concentrations measured in hydrothermal plumes (i.e., up to 90 µg/l; Trocine and Trefry, 1988; Feely et al., 1994).

Interestingly, the shale-normalized REE patterns of these easily leachable sediment fractions are also characterized by a strong positive Ce-anomaly and a marked MREE enrichment (see the theoretical pattern for a non-filtered seawater sample with TSM of 1 mg/l, Fig. 6C). As mentionned earlier, this pattern is typical of sedimentary Fe-oxyhydroxide phases (e.g., Bayon et al., 2004). This suggests that a significant fraction of the REE extracted from our core-top sediments during our leaching experiments is derived from the dissolution of REE-rich Fe-oxyhydroxide phases. By analogy, it is very likely that the measured TDFe, TDMn and TDREE anomalies determined in the non-filtered seawater samples above venting sites were due to dissolution of Fe-Mn oxyhydroxide phases associated to suspended particles within the plumes. Taking a further logical step, we propose that Fe-oxyhydroxide co-precipitation in the near surface environment is responsible for the net removal of pore water REE in sub-surface sediments at active vent sites, thereby leading to the absence of significant emission of dissolved REE into bottom waters.

Interestingly, careful examination of the vertical profiles at both Pockmark Field and Mud Volcano sites shows that dissolved Nd concentrations are actually slightly depleted in methane plumes relative to the overlying water column (Fig. 5). By analogy with what was shown at hydrothermal systems (e.g. Michard et al., 1983; German et al., 1990; Sherrell et al., 1999; Edmonds and German, 2004), this could suggest that additional scavenging of seawater REE take place within the plume, perhaps through continuous adsorption onto Fe-Mn oxyhydroxide phases or any other suspended particulates. Considering the Nd concentrations measured at these two sites (Table 2), one can calculate that Fe-rich particles within the plumes can incorporate up to ~ 7% of the dissolved REE content of ambient seawater. Importantly, this also suggests that fluid seepage at cold seeps could act as a net sink in the global ocean budget of the REE.

4.4. Nd isotope constraints on processes controlling dissolved REE profiles in the Gulf of Guinea

Neodymium isotopic measurements provide further constraints on the processes controlling the distribution of dissolved REE at the studied CTD hydrocast stations. The Nd isotope ratios measured in this study encompass a large range of ε_{Nd} values from about -10.7 to -15.7 (Table 2). Surface waters (TSW) exhibit ε_{Nd} values of ~ -12.5 (CTD08-B13/14, 57m depth), while the underlying subtropical underwater waters (STUW) are characterized by unradiogenic values (~ -15.7; CTD3-B13/14, 60-180m depth). At the transition between South Atlantic central waters and Antarctic Intermediate water, values are centered around ~ -12.5, with the exception of one sample (~ -10.7; CTD06-B10/12, 460-500m depth,). The core of AAIW displays lower ε_{Nd} values (~ -13.3; CTD03-B9/10, 990-1190m depth), while

NADW at the Reference Site is characterized by ε_{Nd} of ~ -12.5. Note that the ε_{Nd} values for the uncleaned foraminifera separates from core-top sediments at the Pockmark Field and Reference sites (Table 5; taken as a indirect measurement of the Nd isotope composition of bottom waters; Roberts and al., 2010) are also in very good agreement with the ε_{Nd} signature determined for deep waters at these sites. Clearly, the large ε_{Nd} variability in the Niger Delta water column indicates various sources of dissolved Nd. Below, we investigate several possible mechanisms (i.e. isotopic exchange at cold seeps, sediment dissolution, lateral advection), which could account for the vertical distribution of Nd isotopes at the three CTD hydrocast stations.

First, although there are clear evidence for a net removal of REE at cold seeps (see previous section), isotopic exchange processes between methane-rich fluids and/or associated particles and seawater could possibly affect the Nd isotopic composition of the Gulf of Guinea bottom waters. To test this hypothesis, we measured the Nd isotopic composition of cold seep carbonate concretions and/or authigenic gypsum from sediments at the Mud Volcano and Pockmark Field, to estimate the ε_{Nd} signature of fluids expelled at these sites. Authigenic gypsum typically forms in reduced sediments after opening of the core sections, as a result of the oxidation of sulfides to sulfate. During precipitation, it probably incorporates a number of dissolved trace element (including REE) from pore waters, and can hence be used to infer the Nd isotopic composition of surrounding pore waters. At the Pockmark Field, the authigenic carbonate concretion exhibits a ε_{Nd} value (-12.0 ± 0.3) similar to the measured bottom water signature (-12.1 ± 0.6), but slightly lower than that for uncleaned foraminifera (-12.5 ± 0.1). At the Mud Volcano, however, the obtained ε_{Nd} values for authigenic minerals (ε_{Nd} from ~ -11.5 to -11.3 ± 0.2; Table 3) differ significantly from that of local bottom waters (-12.3 ± 0.4).

360 In agreement with our REE data, this suggests that fluid seepage at cold seeps do not modify
361 significantly the Nd isotopic composition of bottom water masses at ocean margins.

362

363 Second, as suggested previously for other areas of high sedimentary inputs (Nozaki and
364 Alibo, 2002; Tachikawa et al., 1999), partial dissolution of detrital particles settling through
365 the water column could play a significant role in controlling the vertical distribution of
366 dissolved REE. In the study area, however, both detrital sediments (average ε_{Nd} ~ -11.6 ±
367 0.3) and easily leachable fractions (i.e., dilute HNO_3 leachates; average -11.3 ± 0.3) are
368 characterized by a Nd isotopic signature significantly different from the seawater ε_{Nd} values
369 throughout the water column (Fig. 4). Clearly, this shows that interaction between seawater
370 and settling particles in this part of the Gulf of Guinea is unlikely to play any significant role
371 in the REE oceanic cycling.

372

373 Finally, based on these results, our preferred explanation is that lateral advection (i.e. ocean
374 circulation patterns) controls the observed vertical distribution of Nd isotope ratios at our
375 CTD hydrocast stations. This hypothesis is supported by evidence that 1) each water mass is
376 characterized by a well-distinct ε_{Nd} signature (Fig. 4), and 2) that the composite vertical
377 profile for ε_{Nd} closely resembles those for dissolved Nd concentrations (Fig. 4). In addition,
378 lateral advection would explain well why the Nd isotopic composition for STUW is very
379 unradiogenic (ε_{Nd} ~ -15.7 ± 0.5). In the Gulf of Guinea, the STUW is transported by the
380 northern Equatorial current (Fig. 1), which mainly receives its water from the northward
381 flowing Equatorial undercurrent (EUC). The main rivers draining western equatorial Africa
382 are delivering to the Atlantic Ocean suspended and/or dissolved loads characterized by very
383 low ε_{Nd} values (Congo ~ -16; Allègre et al ., 1996; Bayon et al., 2009; Ogooué ~ -24; G.

384 Bayon, unpubl. data; Ntem ~ -28; Weldeab et al., 2011). Therefore, if any significant
385 sediment/seawater interaction takes place at the western African ocean margin, one would
386 accordingly expect the water masses transported by the EUC to acquire a unradiogenic ε_{Nd}
387 signature, thereby explaining the low value measured in this study for STUW.

388

389 **4.5. Implications for the marine Nd cycle at continental margins**

390 As already mentioned in the Introduction, there are numerous evidence that the Nd isotopic
391 signature of water masses can be modified on ocean margins (e.g. Lacan and Jeandel, 2005;
392 Andersson et al., 2008; Amakawa et al., 2009), which suggest that sediment-seawater
393 interaction at margins could represent a major component of the oceanic Nd cycle (e.g.
394 Arsouze et al., 2009). Similarly, our Nd isotope seawater data for the Niger Delta margin also
395 provide another evidence for 'boundary exchange' (see discussion above for STUW). In
396 addition, the ε_{Nd} value determined for AAIW in our study area (between -13.3 ± 0.3 and -12.4
397 ± 0.4; Table 2) markedly differs from that reported for the same water mass at a nearby
398 station, in the western part of the Gulf of Guinea (-11.5 ± 0.3; Rickli et al., 2010). Similarly
399 to what was proposed above for explaining the unradiogenic signature of STUW, the lower
400 ε_{Nd} value measured here for AAIW most probably indicate sediment/seawater interactions at
401 the western equatorial African margin (Fig. 1). As discussed above, venting of reduced fluids
402 at cold seeps and dissolution of settling lithogenic particles both are unlikely to account for
403 the observed differences. Alternatively, one possible explanation accounting for the shift of
404 AAIW towards unradiogenic ε_{Nd} signature during its northward flow trajectory in this part of
405 the Gulf of Guinea would be that it was modified by diffusive benthic fluxes from organic-
406 rich sediments.

407

Of course, we cannot rule out the possibility that in certain parts of the ocean, dissolution of settling particles, for example, represents the dominant input of dissolved REE to the ocean. Additional case studies would also be clearly needed to confirm the results presented here. However, our data suggest that diffusive benthic fluxes from suboxic settings could represent a substantial source of dissolved REE in the Gulf of Guinea. Earlier works already suggested that diffusion from marine sediments was likely to play a significant role in the marine REE cycle (e.g. Elderfield and Greaves, 1982). Although only few studies have examined the distribution of REE in interstitial waters of marine sediments (Elderfield and Sholkovitz, 1987; Sholkovitz et al., 1989; Haley et al., 2004), these works clearly showed that REE were significantly enriched in pore waters relative to bottom waters, in agreement with the data presented here, establishing strong chemical gradients in the near surface environment. Certainly, the relatively high REE contents in pore waters are derived from the degradation of potentially REE-rich phases (e.g., organic material, Fe-Mn oxyhydroxides) during early diagenetic processes (e.g. Haley et al., 2004), which, in turn, is closely related to the amount of organic compounds accumulated in subsurface sediments. As a first approximation, therefore, one could suggest that the benthic fluxes of dissolved REE from marine sediments are positively correlated with organic material contents. Because accumulation rates of organic material in marine sediments are typically much higher on continental margins than in open ocean settings, this would be entirely consistent with the proposed hypothesis that sediment-seawater interactions at margins (in this case, benthic fluxes from suboxic sediments) may represent a important component of the marine Nd cycle.

4 – Conclusion

The data presented here indicate that seepage of methane-rich fluids on continental margins do not represent a source of dissolved Nd to the ocean. Similarly to what was previously

reported at submarine hydrothermal systems, it is very likely that Fe-Mn oxyhydroxide precipitation in sub-surface sediments leads to quantitative removal of dissolved REE whenever reduced (anoxic) fluids are emitted at cold seeps, acting possibly as a net sink for REE in the ocean. In contrast, we suggest that diffusive benthic fluxes from suboxic surface sediments could play a significant role in the marine Nd cycle, at least at the Niger Delta margin.

Acknowledgments

We thank the Captains, the officers and crews of R/V *Pourquoi Pas?*, and members of the ERIG-3D scientific parties for their assistance at sea. We are very grateful to the three anonymous reviewers for their thoughtful and constructive comments, and thanks G.M. Henderson for editorial handling. This work was funded by IFREMER and TOTAL via the ERIG-3D project.

References

Allègre, C.J., Dupré, B., Negrel, P., Gaillardet, J., 1996. Sr-Nd-Pb isotope systematics in Amazon and Congo River systems: Constraints about erosion processes. Chem. Geol. 131, 93-112.

Amakawa, H., Alibo, D.S., Nozaki, Y., 2000. Nd isotopic composition and REE pattern in the surface waters of the eastern Indian Ocean and its adjacent seas. Geochim. Cosmochim. Acta 64, 1715–1727.

Amakawa, H., Sasaki, K., Ebihara, M., 2009. Nd isotopic composition in the central North Pacific. Geochim. Cosmochim. Acta 73, 4705–4719.

457 Andersson, P.S., Porcelli, D., Frank, M., Bjork, G., Dahlqvist, R., Gustafsson, O., 2008.
458 Neodymium isotopes in seawater from the Barents Sea and Fram Strait Arctic-Atlantic
459 gateways. Geochim. Cosmochim. Acta 72, 2854–2867.
460 Arsouze, T., Dutay, J.-C., Lacan, F., Jeandel, C., 2009. Reconstructing the Nd oceanic cycle
461 using a coupled dynamical – biogeochemical model. Biogeosciences, 6, 5549-5588.
462 Arsouze, T., Dutay, J.-C., Lacan, F., Jeandel, C., 2007. Modeling the neodymium isotopic
463 composition with a global ocean general circulation model. Chem. Geol. 239, 156–164.
464 Barrat, J.A., Keller, F., Amossé, J., Taylor, R.N., Nesbitt, R.W., Hirata, T., 1996.
465 Determination of rare earth element in sixteen silicate reference samples by ICP-MS after
466 Tm addition and ion exchange separation. Geostand. Newslett. 20, 133-139.
467 Bayon, G., German, C.R., Boella, R.M. Milton, J.A. Taylor, R.N. Nesbitt, R.W., 2002. Sr and
468 Nd isotope analyses in paleoceanography: the separation of both detrital and Fe–Mn
469 fractions from marine sediments by sequential leaching. Chem. Geol. 187, 179–199.
470 Bayon, G., German, C.R., Burton, K.W., Nesbitt, R.W., Rogers, N., 2004. Sedimentary Fe–
471 Mn oxyhydroxides as paleoceanographic archives and the role of aeolian flux in regulating
472 oceanic dissolved REE. Earth Planet. Sci. Lett. 224, 477–492.
473 Bayon, G., Pierre, C., Etoubleau, J., Voisset, M., Cauquil, E., Marsset, T., Sultan, N., Le
474 Drezen, E., Fouquet, Y., 2007. Sr/Ca and Mg/Ca ratios in Niger Delta sediments:
475 Implications for authigenic carbonate genesis in cold seep environments. Mar. Geol. 241,
476 93-109.
477 Bayon, G., Barrat, J.-A., Etoubleau, J., Benoit, M., Bollinger, C., Révillon, S., 2009a.
478 Determination of rare earth elements, Sc, Y, Zr, Ba, Hf and Th in geological samples by
479 ICP-MS after Tm addition and alkaline fusion. Geostand. Geoanal. Res. 33, 51-62.

480 Bayon, G., Burton, K.W., Soulet, G., Vigier, N., Dennielou, B., Etoubleau, J., Ponzevera, E.,
481 German, C.R., Nesbitt, R.W., 2009b. Hf and Nd isotopes in marine sediments: Constraints
482 on global silicate weathering. Earth Planet. Sci. Lett. 277, 318-326.
483 Bayon, G., Birot, D., Bollinger, C., Barrat, J.A., 2011. Multi-elemental analyses of trace
484 metals in seawater by ICP-SFMS after Tm addition and iron co-precipitation. Geostand.
485 Geoanal. Res. 35, 145-153.
486 Bertram, C.J., Elderfield, H., 1993. The geochemical balance of the rare earth elements and
487 neodymium isotopes in the oceans, Geochim. Cosmochim. Acta 57, 1957–1986.
488 Brooks, J.M., Anderson, A.L., Sassen, R., MacDonald, I.R., Kennicutt, II M.C., Guinasso Jr.,
489 N.L., 1994. Hydrate occurrences in shallow subsurface cores from continental slope
490 sediments. In: Annals of the New York Academy of Sciences 715, 381-391.
491 Castellini, D.G., Dickens, G.R., Snyder, G.T., Ruppel, C.D., 2006. Barium cycling in shallow
492 sediment above active mud volcanoes in the Gulf of Mexico. Chem. Geol. 226, 1-30.
493 Charlou, J.L., Donval, J.P., 1993. Hydrothermal methane venting between 12°N and 26°N
494 along the Mid-Atlantic Ridge. J. Geophys. Res. 98, 9625-9642.
495 Charlou, J.L., Fouquet, Y., Bougault, H., Donval, J.P., Etoubleau, J., Jean-Baptiste, P.,
496 Dapoigny, A., Appriou, P., Rona, P.A., 1998. Intense CH4 plumes generated by
497 serpentinization of ultramafic rocks at the intersection of the 15°20’N fracture zone and the
498 Mid-Atlantic Ridge. Geochim. Cosmochim. Acta 62, 2323-2333.
499 Charlou, J.L., Donval, J.P., Fouquet, Y., Ondreas, H., Knoery, J., Cochonat, P., Levaché, D.,
500 Poirier, Y., Jean-Baptiste, P., Fourré, E., Chazallon, B., The ZAIROV Leg 2 Scientific
501 Party, 2004. Physical and chemical characterization of gas hydrates and associated
502 methane plumes in the Congo–Angola Basin. Chem. Geol. 205, 405-425.
503 Cohen, H.A., McClay, K., 1996. Sedimentation and shale tectonism of the southwestern Niger
504 Delta front. Mar. Petrol. Geol. 13, 313-329.

505 DePaolo, D.J., Wasserburg, G.J., 1976. Nd isotopic variations and petrogenetic models.
506 Geophys. Res. Lett. 3, 249-252.
507 Edmonds, H.N., German, C.R., 2004. Particle geochemistry in the Rainbow hydrothermal
508 plume, Mid-Atlantic Ridge. Geochim. Cosmochim. Acta 68, 759-772.
509 Elderfield, H., Greaves, M.J., 1982. The rare-earth elements in sea-water. Nature 296, 214-
510 219.
511 Elderfield, H., Sholkovitz, E.R., 1987. Rare earth elements in the pore waters of reducing
512 nearshore sediments. Earth Planet. Sci. Lett. 82, 280–288.
513 Elderfield, H., UpstillGoddard, R., Sholkovitz, E.R., 1990. The rare-earth elements in rivers,
514 estuaries, and coastal seas and their significance to the composition of ocean waters.
515 Geochim. Cosmochim. Acta 54, 971-991.
516 Feely, R.A., Gendron, J.F., Baker, E.T., Lebon, G.T., 1994. Hydrothermal plumes along the
517 East Pacific Rise, 8°40' to 11°50'N – particle composition and distribution. Earth Planet.
518 Sci. Lett. 128, 19-36.
519 Frank, M., 2002. Radiogenic isotopes: tracers of past ocean circulation and erosional input.
520 Rev. Geophys. 40, doi :10.1029/2000RG000094.
521 Freslon, N., Bayon, G., Birot, D., Bollinger, C., Barrat, J.A., 2011. Determination of rare
522 earth elements and other trace elements (Y, Mn, Co, Cr) in seawater using Tm addition and
523 $Mg(OH)_2$ co-precipitation. Talanta, 85, 582-587.
524 Froelich, P.N., Klinkhammer, G.P., Bender, M.L., Luedtke, N.A., Heath, G.R., Cullen, D.,
525 Dauphin, P., Hammond, D. and Hartman, B., 1979. Early oxidation of organic matter in
526 pelagic sediments of the eastern equatorial Atlantic - suboxic diagenis. Geochim.
527 Cosmochim. Acta 43, 1075-1090.
528 German, C.R., Elderfield, H., 1990. Rare earth elements in the NW Indian Ocean. Geochim.
529 Cosmochim. Acta 54, 1929-1940.

530 German, C.R., Klinkhammer, G.P., Edmond, J.M., Mitra, A., Elderfield, H., 1990.
531 Hydrothermal scavenging of rare earth elements in the ocean. Nature 345, 516-518.
532 Goldstein, S.J., Jacobsen, S.J., 1987. The Nd and Sr isotopic systematics of river-water
533 dissolved material: Implications for the sources of Nd and Sr in seawater. Chem. Geol. 66,
534 245-272.
535 Goldstein, S.L., Hemming, S.R., 2003. Long-lived isotopic tracers in oceanography,
536 paleoceanography, and ice-sheet dynamics. In: H. Elderfield, Editor, Treatise on
537 Geochemistry, Elsevier, Oxford.
538 Greaves, M.J., Statham, P.J., Elderfield, H., 1994. Rare earth element mobilization from
539 marine atmospheric dust into seawater. Mar. Chem. 46, 255–260.
540 Gutjahr, M., Frank, M., Stirling, C.H., Keigwin, L.D., Halliday, A.N., 2008. Tracing the Nd
541 isotope evolution of North Atlantic deep and intermediate waters in the Western North
542 Atlantic since the Last Glacial Maximum from Blake Ridge sediments. Earth Planet. Sci.
543 Lett. 266, 61-77.
544 Haley, B.A., Klinkhammer, G.P., McManus, J., 2004. Rare earth elements in pore waters of
545 marine sediments. Geochim. Cosmochim. Acta 68, 1265-1279.
546 Haley, B.A., Frank, M., Spielhagen, R.F., Eisenhauer, A., 2008. Influence of brine formation
547 on Arctic Ocean circulation over the past 15 million years. Nature Geosci. 1, 68-72.
548 Halliday, A.N., Davidson, J.P., Holden, P., Owen, R.M., Olivarez, A.M., 1992. Metalliferous
549 sediments and the scavenging residence time of Nd near hydrothermal vents. Geophys.
550 Res. Lett. 19, 761–764.
551 Hovland, M., Judd, A.G., 1992. The global production of methane from shallow marine
552 sources. Cont. Shelf Res. 12, 1209-1218.
553 Jacobson, A.D., Holmden, C., 2006. Calcite dust and the atmospheric supply of Nd to the
554 Japan Sea. Earth Planet. Sci. Lett. 244, 418-430.

555 Jeandel, C., Thouron, D., Fieux, M., 1998. Concentrations and isotopic compositions of
556 neodymium in the eastern Indian Ocean and Indonesian straits. Geochim. Cosmochim.
557 Acta 62, 2597-2607.
558 Johannesson, K.H., Burdige, D.J., 2007. Balancing the global oceanic neodymium budget:
559 evaluating the role of groundwater. Earth Planet. Sci. Lett. 253,129–142.
560 Judd, A.G., Hovland, M., Dimitrov, L.I., Gil, S.G., Jukes, V., 2002. The geological methane
561 budget at continental margins and its influence of climate change. Geofluids 2, 109-
562 126.
563 Kopf, A., 2003. Global methane emission through mud volcanoes and its past and present
564 impact on the Earth's climate. Int. J. Earth Sci. (Geol. Rundsch.) 92, 806-816.
565 Lacan, F., Jeandel, C., 2001. Tracing Papua New Guinea imprint on the central Equatorial
566 Pacific Ocean using neodymium isotopic compositions and Rare Earth Element
567 patterns. Earth Planet. Sci. Lett. 186, 497–512.
568 Lacan, F., Jeandel, C., 2004a. Denmark Strait water circulation traced by heterogeneity in
569 neodymium isotopic compositions. Deep-Sea Res. I 51, 71-82.
570 Lacan, F., Jeandel, C., 2004b. Neodymium isotopic composition and rare earth element
571 concentrations in the deep and intermediate Nordic Seas: Constraints on the Iceland
572 Scotland Overflow Water signature. Geochem. Geophys. Geosys. 5, Q11006.
573 Lacan, F., Jeandel, C., 2005. Neodymium isotopes as a new tool for quantifying exchange
574 fluxes at the continent-ocean interface. Earth Planet. Sci. Lett. 232, 245–257.
575 Mascle, J., Bornhold, B.D., Renard, V. 1973. Diapiric structures off Niger delta. Amer.
576 Assoc. Petrol. Geol. Bull. 57, 1672-1678.
577 McQuay, E.L., Torres, M.E., Collier, R.W., Huh, C.A., McManus, J., 2008. Contribution of
578 cold seep barite to the barium geochemical budget of a marginal basin. Deep-Sea Res. I
579 55, 801-811.

Michard, A., Albarède, F., Michard, G., Minster, J.F., Charlou J.L., 1983. Rare-earth elements and uranium in high-temperature solutions from East Pacific Rise hydrothermal vent field (13 °N). Nature 303, 795-797.

Milkov, A.V., Sassen, R., Apanasovich, T.V., Dadashev, F.G., 2003. Global gas flux from mud volcanoes: a significant source of fossil methane in the atmosphere and the ocean. Geophys. Res. Lett. 30, 1037, doi:10.1029/2002GL0165358.

Nozaki, Y., Alibo, D.S., 2003. Importance of vertical geochemical processes in controlling the oceanic profiles of dissolved rare earth elements in the northeastern Indian Ocean. Earth Planet. Sci. Lett. 205, 155-172.

Piotrowski, A.M., Goldstein, S.L., Hemming, S.R., Fairbanks, R.G., 2005. Temporal relationships of carbon cycling and ocean circulation at glacial boundaries. Science 307, 1933–1938.

Piotrowski, A.M., Banakar, V.K., Scrivner, A.E., Elderfield, H., Galy, A., Dennis, A., 2009. Indian Ocean circulation and productivity during the last glacial cycle. Earth Planet. Sci. Lett. 285, 179-189.

Puceat, E., Lecuyer, C., Reisberg, L., 2005. Neodymium isotope evolution of NW Tethyan upper ocean waters throughout the Cretaceous. Earth Planet. Sci. Lett. 236, 705-720.

Original Research Article

Rickli, J., Frank, M., Baker, A.R., Aciego, S., de Souza, G., Georg, R.B., Halliday, A.N., 2010. Hafnium and neodymium isotopes in surface waters of the eastern Atlantic Ocean: Implications for sources and inputs of trace metals to the ocean. Geochim. Cosmochim. Acta 74, 540-557.

Roberts, N.L., Piotrowski, A.M., McManus, J.F., Keigwin, L.D., 2010. Synchronous Deglacial Overturning and Water Mass Source Changes. Science 327, 75-78.

604 Robinson, L.F., van de Flierdt, T., 2009. Southern Ocean evidence for reduced export of
605 North Atlantic Deep Water during Heinrich event 1. Geology 37, 195-198.
606 Rongemaille, E., Bayon, G., Pierre, C., Bollinger, C., Chu, N.C., Favreau, E., Fouquet, Y.,
607 Riboulot, V., Voisset, M., 2011. Rare earth elements in cold seep carbonates from the
608 Niger Delta. Chem. Geol. 286, 196-206.
609 Rutberg, R.L., Hemming, S.R., Goldstein, S.L., 2000. Reduced North Atlantic Deep Water
610 flux to the glacial Southern Ocean inferred from neodymium isotope ratios. Nature 405,
611 935–938.
612 Scher, H.D., Martin, E.E., 2004. Circulation in the Southern Ocean during the Paleogene
613 inferred from neodymium isotopes. Earth Planet. Sci. Lett. 228, 391–405.
614 Sherrell, R.M., Field, M.P., Ravizza, G., 1999. Uptake and fractionation of rare earth
615 elements on hydrothermal plume particles at 9 degrees 45 ' N, East Pacific Rise. Geochim.
616 Cosmochim. Acta 63, 1709-1722.
617 Sholkovitz, E.R., 1995. The aquatic chemistry of rare earth elements in rivers and estuaries.
618 Aquat. Geochem. 1, 1–34.
619 Sholkovitz, E.R., Szymczak, R., 2000. The estuarine chemistry of rare earth elements:
620 comparison of the Amazon, Fly, Sepik and the Gulf of Papua systems. Earth Planet. Sci.
621 Lett. 179, 299–309.
622 Sholkovitz, E.R., Piepgras, D.J., Jacobsen, S.B., 1989. The pore water chemistry of rare earth
623 elements in Buzzards Bay sediments. Geochim. Cosmochim. Acta 53, 2847–2856.
624 Sholkovitz, E.R., Shaw, T.J., Schneider, D.L., 1992. The geochemistry of rare earth elements
625 in the seasonally anoxic water column and porewaters of Chesapeake Bay. Geochim.
626 Cosmochim. Acta 56, 3389-3402.
627 Sholkovitz, E.R., Elderfield, H., Szymczak, R., Casey, K., 1999. Island weathering: river
628 sources of rare earth elements to the Western Pacific Ocean, Mar. Chem. 68, 39–57.

629 Sultan, N., Voisset, M., Marsset, B., Marsset, T., Cauquil, E., Colliat, J.L., 2007. Potential
630 role of compressional structures in generating submarine slope failures in the Niger Delta.
631 Mar. Geol. 237, 169-190.
632 Sultan, N., Marsset, B., Ker, S., Marsset, T., Voisset, M., Vernant, A.M., Bayon, G., Cauquil,
633 E., Adamy, J., Colliat, J.L., Drapeau, D., 2010. Hydrate dissolution as a potential
634 mechanism for pockmark formation in the Niger delta. J. Geophys. Res 115, B08101.
635 Tachikawa, K., Jeandel, C., Roy-Barman, M., 1999. A new approach to Nd residence time:
636 The role of atmospheric inputs. Earth Planet. Sci. Lett. 170, 433–446.
637 Tachikawa, K., Athias, V., Jeandel, C., 2003. Neodymium budget in the modern ocean and
638 paleo-oceanographic implications. J. Geophys. Res. 108, 3254, doi
639 :10.1029/1999JC000285.
640 Thomson, J., Higgs, N.C., Croudace, I.W., Colley, S. Hydes, D.J., 1993. Redox zonation of
641 elements at an oxic/post-oxic boundary in deep-sea sediments. Geochim. Comochim. Acta
642 57, 579-595.
643 Torres, M.E., Bohrmann, G., Suess, E., 1996. Authigenic barites and fluxes of barium
644 associated with fluid seeps in the Peru subduction zone. Earth Planet. Sci. Lett. 144, 469–
645 481.
646 Torres, M.E., McManus, J., Huh, C.A., 2002. Fluid seepage along the San Clemente Fault
647 scarp: basin-wide impact on barium cycling. Earth Planet. Sci. Lett. 203, 181–194.
648 Trocine, R.P., Trefry, J.H., 1988. Distribution and chemistry of suspended particles from an
649 active hydrothermal vent site on the Mid-Atlantic Ridge at 26°N. Earth Planet. Sci. Lett.
650 88, 1-15.
651 van de Flierdt, T., Robinson, L.F., Adkins, J.F., Hemming, S.R., Goldstein, S.L., 2006.
652 Temporal stability of the neodymium isotope signature of the Holocene to glacial North
653 Atlantic. Paleoceanography 21, PA4102, doi: 10.1029/2006PA001294.

Wallmann, K., Drews, M., Aloisi, G., Bohrmann, G., 2006. Methane discharge into the Black Sea and the global ocean via fluid flow through submarine mud volcanoes. Earth Planet. Sci. Lett. 248, 545-560.

Weldeab, S., Frank, M., Stichel, T., Haley, B., Sangen, M., 2011. Spatio-temporal evolution of the West African monsoon during the last deglaciation. Geophys. Res. Lett. 38, L13703, doi: 10.1029/2011GL047805.

Figure captions

Figure 1. Location of the three studied areas on the Niger Delta margin.

Location map showing the location of the study areas in the Gulf of Guinea. GC (Guinea Current) transports Tropical Surface Water (TSW) eastward in the Gulf of Guinea, whereas STUW (Subtropical Underwater) is advected by EUC (Equatorial Undercurrent) and NSEC (Northern Equatorial Current), respectively. NICC (Northern Intermediate Countercurrent) transports AAIW (Antarctic Intermediate Water) in the study area.

Figure 2. Shaded bathymetric map for the Pockmark Field and the Mud Volcano areas.

The location of the hydrocast stations and studied sediment cores is represented with large white circles and small red circles, respectively. A) The pockmark field area is characterized by the presence of large seafloor depressions with irregular shapes. B) The studied mud volcano (about 1km wide) is composed of two distinct volcanic cones. Note the presence of a well-characterized depression at the periphery of the mud volcano.

Figure 3. Hydrography at the Niger Delta margin.

A) Salinity versus depth profiles and B) Temperature-Salinity diagram for the three studied hydrocast stations. The positions corresponding to the seawater samples analysed for Nd isotopes are shown in the Temperature-Salinity diagram. TSW: Tropical Surface Water; STUW: Subtropical Underwater; SACW: South Atlantic Central Water; AAIW: Antarctic Intermediate Water; NADW: North Atlantic Deep Water (NADW).

Figure 4. Depth profiles for methane, total dissolvable (TD) concentrations for Mn, Fe and Nd, dissolved Nd and ε_{Nd}.

The methane, TDFe and TDMn concentrations show that active fluid venting occurs at the Pockmark Field and Mud volcano sites, with methane plumes rising up to about 100 m above the seafloor. Note that ε_{Nd} represents the relative deviation of the $^{143}Nd/^{144}Nd$ ratios of a sample, in parts per 10^4, from that of the CHUR reference (CHondritic Uniform Reservoir): $[(^{143}Nd/^{144}Nd)_{sample} / (^{143}Nd/^{144}Nd)_{CHUR} -1] \times 10^4$. The average Nd isotopic composition of leachable and detrital sediment fractions from Niger Delta core-top sediments is shown for comparison.

Figure 5. Relationships between total dissolvable (TD) and dissolved Nd concentrations in the bottom part of the water column.

The TDNd concentrations at the Pockmark Field and Mud volcano stations are significantly enriched in the methane plumes. In contrast, dissolved Nd contents for the same samples are much lower, and do not exhibit any significant enrichment relative to the overlying water column. In the upper panel (Pockmark Field), note the small depletion in dissolved Nd at the bottom part of the plume relative to the upper part.

Figure 6. Shale-normalised REE patterns for seawater (both non-filtered and filtered) and pore water samples.

A) At the Pockmark Field, filtered samples collected from within the plume exhibit similar shale-normalized patterns, while non-filtered samples collected at the same water depths show a large range of REE patterns. B) At the Reference site, in contrast, both filtered and non-filtered samples display similar REE patterns. C) Theoretical REE patterns generated by partial dissolution of sediments in seawater samples having total suspended matter loadings (TSM) of about 0.1, 0.2 and 1 mg/l. The theoretical REE concentra are generated using simple mass balance calculations with REE concentrations for typical bottom water (filtered sample CTD08-B3) and the easily leachable fraction of core ER-CS-38.

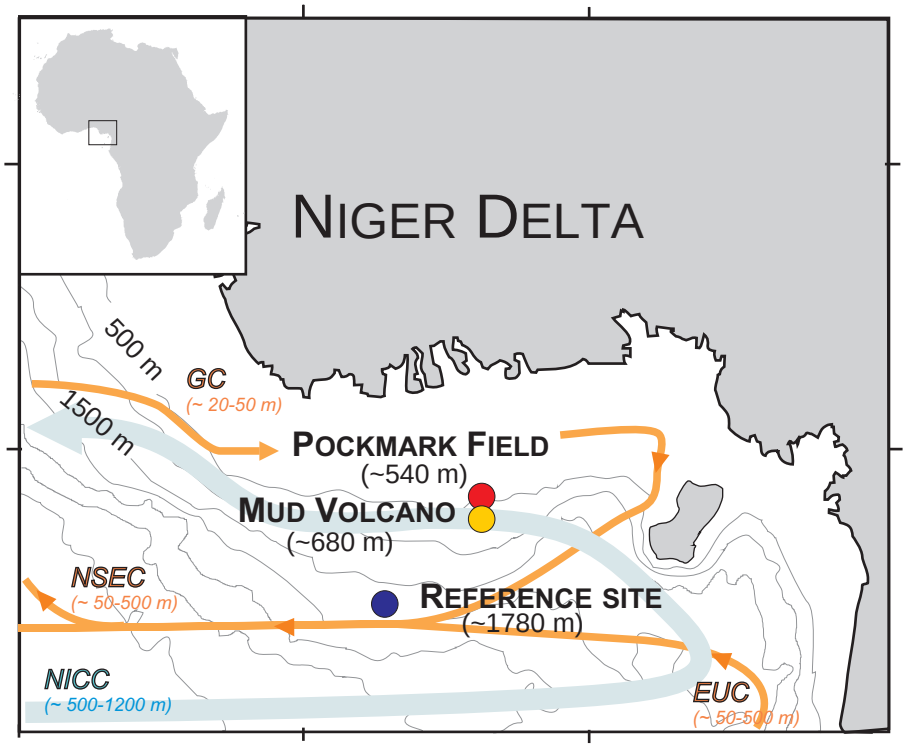
NIGER DELTA
500 m
1500 m
GC
(~ 20-50 m)
POCKMARK FIELD
(~540 m)
MUD VOLCANO
(~680 m)
NSEC
(~ 50-500 m)
REFERENCE SITE
(~1780 m)
NICC
(~ 500-1200 m)
EUC
(~ 50-500 m)

Fig. 1

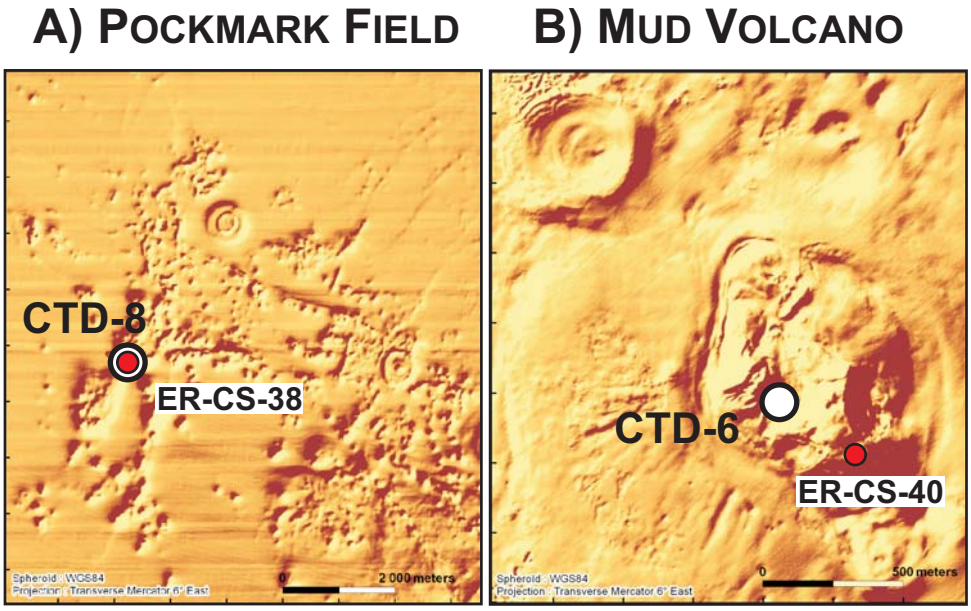
A) POCKMARK FIELD
B) MUD VOLCANO
CTD-8
ER-CS-38
Spheroid: WGS84
Projection: Transverse Mercator 6° East
0
2 000 meters
CTD-6
ER-CS-40
Spheroid: WGS84
Projection: Transverse Mercator 6° East
0
500 meters

Fig. 2

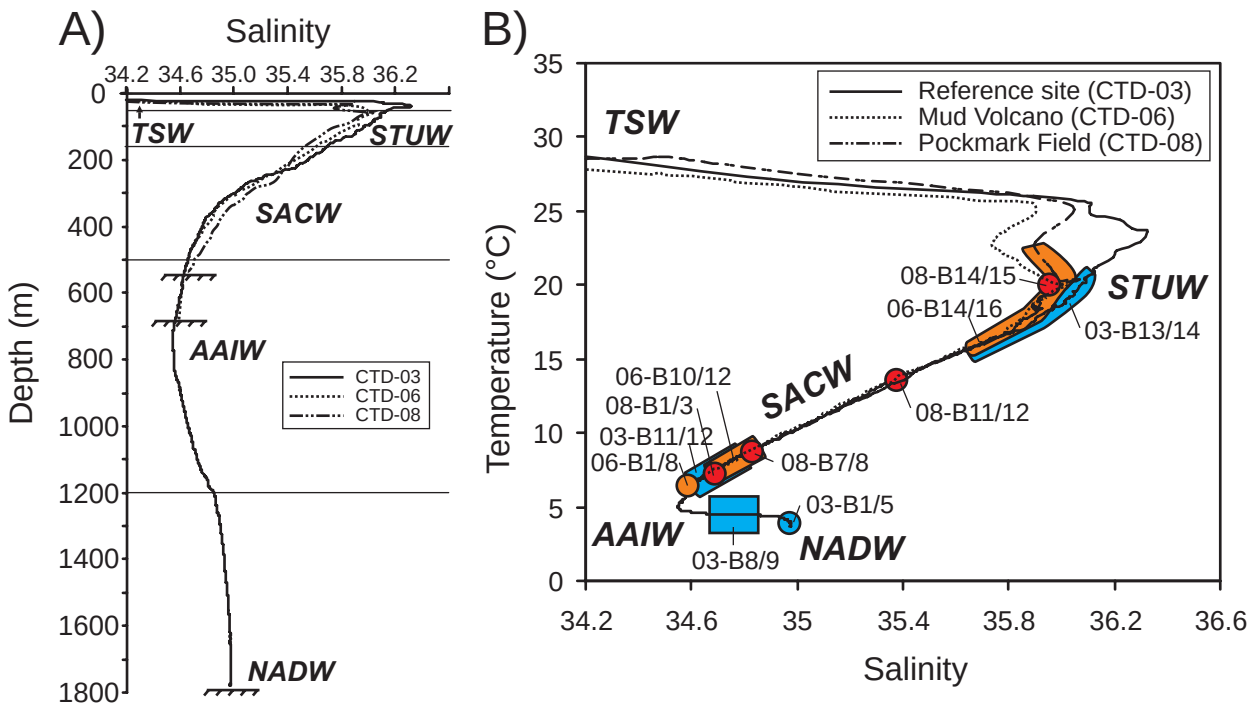
A)
Salinity
34.2 34.6 35.0 35.4 35.8 36.2
0
200
400
600
800
1000
1200
1400
1600
1800
Depth (m)
TSW
STUW
SACW
AAIW
NADW
CTD-03
CTD-06
CTD-08
B)
35
30
25
20
15
10
5
0
Temperature (°C)
34.2
34.6
35
35.4
35.8
36.2
36.6
Salinity
Reference site (CTD-03)
Mud Volcano (CTD-06)
Pockmark Field (CTD-08)
TSW
STUW
SACW
AAIW
NADW
08-B14/15
06-B14/16
03-B13/14
06-B10/12
08-B1/3
03-B11/12
06-B1/8
08-B7/8
08-B11/12
03-B1/5
03-B8/9

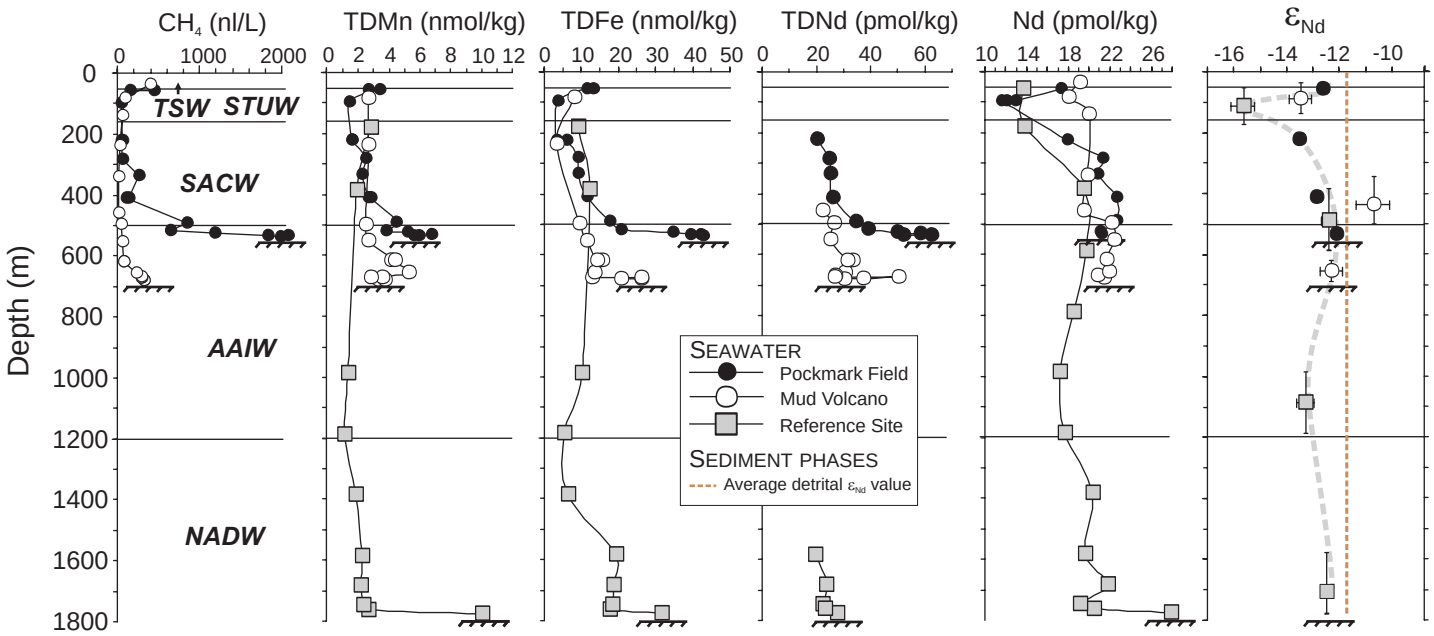
CH4 (nl/L)
TDMn (nmol/kg)
TDFe (nmol/kg)
TDNd (pmol/kg)
Nd (pmol/kg)
εNd
Depth (m)
TSW STUW
SACW
AAIW
NADW
SEAWATER
Pockmark Field
Mud Volcano
Reference Site
SEDIMENT PHASES
Average detrital εNd value

Fig. 4

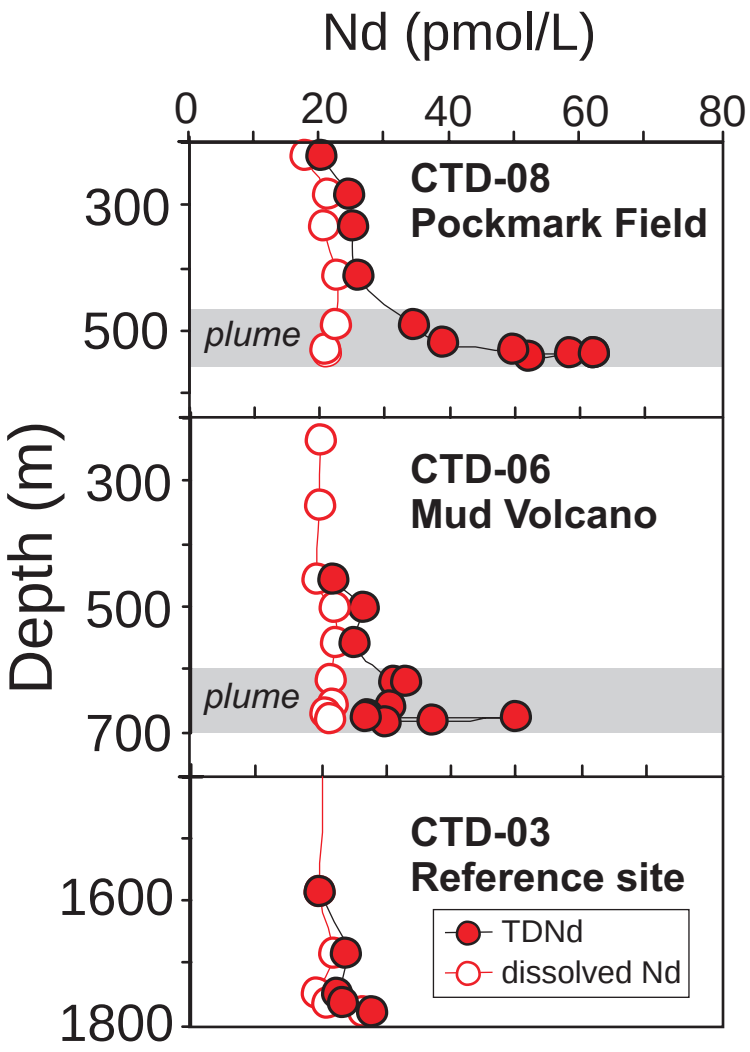
Nd (pmol/L)
0
20
40
60
80
Depth (m)
300
500
plume
CTD-08
Pockmark Field
300
500
700
plume
CTD-06
Mud Volcano
1600
1800
CTD-03
Reference site
TDNd
dissolved Nd

Fig. 5

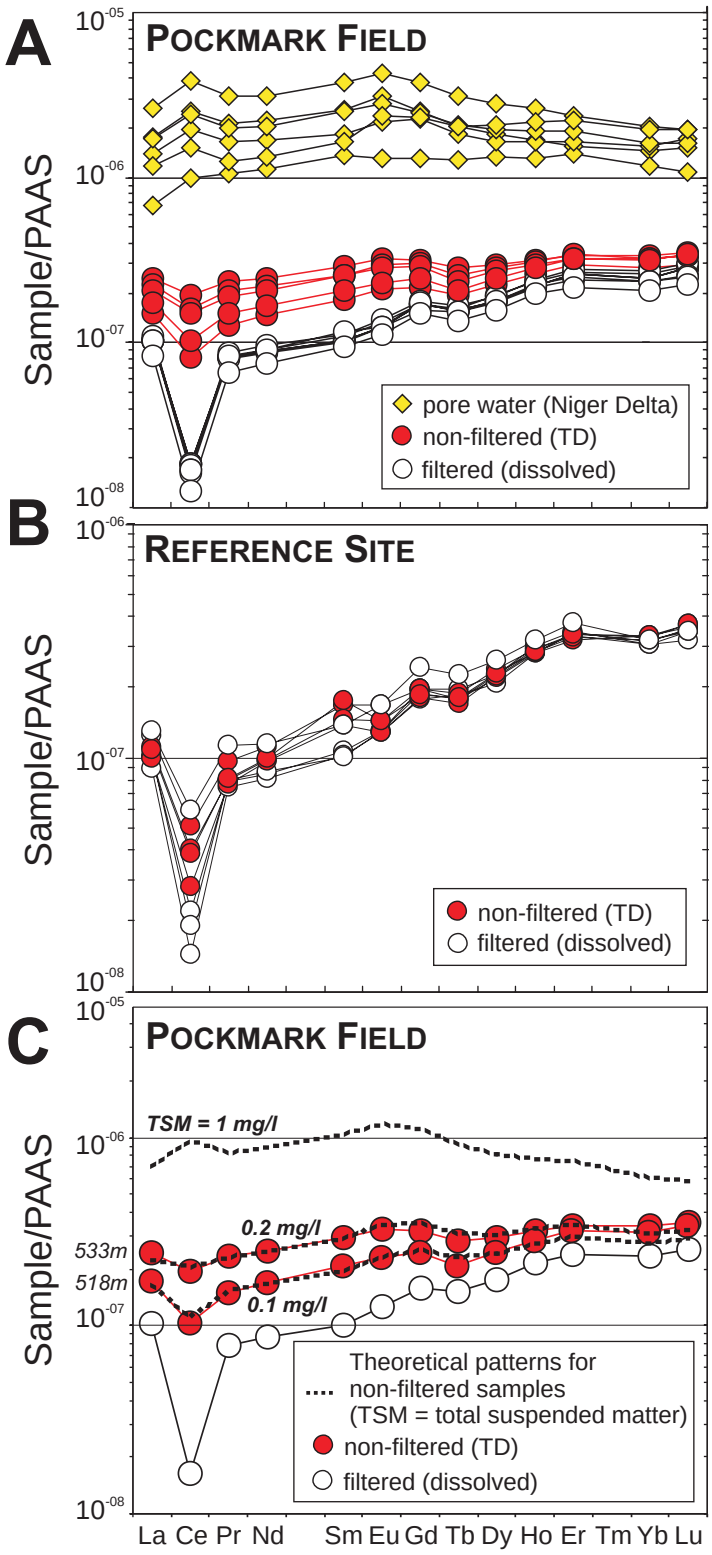
A
POCKMARK FIELD
Sample/PAAS
10-05
10-06
10-07
10-08
pore water (Niger Delta)
non-filtered (TD)
filtered (dissolved)
B
REFERENCE SITE
Sample/PAAS
10-06
10-07
10-08
non-filtered (TD)
filtered (dissolved)
C
POCKMARK FIELD
Sample/PAAS
TSM = 1 mg/l
0.2 mg/l
533m
518m
0.1 mg/l
10-05
10-06
10-07
10-08
Theoretical patterns for
non-filtered samples
(TSM = total suspended matter)
non-filtered (TD)
filtered (dissolved)
La Ce Pr Nd Sm Eu Gd Tb Dy Ho Er Tm Yb Lu

Fig. 6

Tables

Table 1
CH_4 and total dissolvable concentrations (Mn, Fe, REE) for Niger Delta seawater samples.

Sample	Depth	CH_4	Mn	Fe	La	Ce	Pr	Nd	Sm	Eu	Gd	Tb	Dy	Ho	Er	Yb	Lu
	(m)	(nl/l)	(nmol/kg)	(nmol/kg)	(pmol/kg)												
ER-CTDR-03 — Reference Area																	
CTD3-B1	1776		10.28	30.23	34.72	29.02	6.08	26.41	6.44	1.21	3.00	0.92	6.97	1.77	5.82	5.37	0.93
CTD3-B2	1762		2.41	18.46	30.70	23.23	5.06	23.24	5.56	1.03	2.81	0.87	6.41	1.69	5.48	5.42	0.91
CTD3-B3	1747		2.07	19.09	27.38	16.12	4.84	22.56	5.39	0.92	2.04	0.84	6.43	1.72	5.60	5.22	0.88
CTD3-B4	1682		1.82	19.24	30.11	22.31	5.14	23.62	6.55	1.03	2.36	0.89	6.63	1.72	5.79	5.43	0.92
CTD3-B6	1585		1.92	19.93	27.58	14.86	4.46	19.80	4.60	1.00	5.13	0.80	6.26	1.65	5.69	5.37	0.91
CTD3-B7	1385		1.46	8.97													
CTD3-B8	1187		0.73	7.99													
CTD3-B9	987		0.99	12.08													
CTD3-B12	385		1.59	13.93													
CTD3-B13	181		2.54	11.34													
ER-CTDR-06 — Mud Volcano																	
CTD6-B1	679	327	3.06	20.94	34.85	25.19	6.85	30.16	5.54	1.23	5.66	0.86	6.00	1.49	4.96	4.75	0.74
CTD6-B2	679	317	3.53	25.50	43.20	48.79	8.36	37.16	6.76	1.33	2.96	0.96	6.81	1.68	5.10	4.76	0.86
CTD6-B3	673	300	3.36	25.45	40.92	43.10	11.50	50.12	7.41	1.41	2.32	0.99	7.59	1.58	5.09	4.96	0.84
CTD6-B4	673	289	2.58	14.35	40.80	25.87	6.02	27.07	5.56	1.08	1.91	0.86	5.94	1.53	4.73	4.45	0.80
CTD6-B5	668	287	3.65		33.39	26.69	6.17	27.04	5.88	1.20	1.95	0.82	5.63	1.47	4.80	4.71	0.79
CTD6-B6	658	239	5.21	14.84	34.90	26.98	6.88	30.67	5.65	1.13	1.99	0.85	6.18	1.51	4.97	4.54	0.86
CTD6-B7	618	73	3.98	16.74	42.63	45.63	7.89	33.15	6.68	1.46	3.40	0.93	6.44	1.61	5.28	5.05	0.88
CTD6-B8	618	80	4.22	15.48	41.59	36.90	7.19	31.29	6.82	1.30	2.59	0.89	6.28	1.59	5.21	4.87	0.82
CTD6-B9	553	58	2.36	13.24	31.91	23.53	5.54	25.27	5.00	1.12	2.27	0.74	5.62	1.43	4.82	4.64	0.80
CTD6-B10	498	53	2.22	11.51	33.38	26.41	6.09	26.70	6.16	1.14	1.82	0.80	5.77	1.54	4.79	4.58	0.77
CTD6-B11	458	16	1.89		29.13	17.62	4.84	22.00	4.95	0.99	1.64	0.74	5.56	1.44	4.67	4.34	0.72
CTD6-B12	340	22															
CTD6-B13	239	33	2.41	6.52													
CTD6-B14	141	63															
CTD6-B15	84	95	2.34	10.29													
CTD6-B16	38	410															
ER-CTDR-08 — Pockmark Field																	
CTD8-B2	537	2088	5.58	39.65	61.43	90.55	12.94	52.20	9.61	2.12	5.64	1.25	8.12	1.84	5.90	5.30	0.84
CTD8-B1	535	1984	5.85	36.54	180.6	114.6	17.93	62.20	10.97	2.09	6.63	1.32	8.31	1.99	6.10	5.46	0.92
CTD8-B3	533	1838	6.76	38.91	67.66	110.6	14.65	58.53	10.93	2.30	5.87	1.37	8.55	1.90	5.78	5.54	0.88
CTD8-B4	525	1195	5.10	32.68	56.55	86.24	11.88	49.83	9.38	2.00	5.04	1.15	7.91	1.77	5.51	5.23	0.83
CTD8-B5	518	648	3.58	20.84	47.69	58.29	9.36	39.09	7.78	1.64	3.49	1.02	7.03	1.70	5.47	5.14	0.85
CTD8-B6	490	856	4.31	18.33	41.49	46.18	7.97	34.68	6.78	1.50	2.25	0.95	6.46	1.59	5.05	4.61	0.74
CTD8-B7	411	119	2.60	18.52	34.40	21.51	5.97	26.14	5.35	1.10	9.52	0.78	5.64	1.44	4.42	4.33	0.73
CTD8-B8	411	126	2.41	13.31													
CTD8-B9	335	276	1.95	11.38	32.21	19.78	5.41	25.19	4.73	1.15	1.58	0.75	5.63	1.35	4.40	3.97	0.65
CTD8-B10	283	63	2.21	11.31	31.65	20.90	5.44	24.66	5.37	1.16	6.79	0.76	5.49	1.35	4.28	3.88	0.65
CTD8-B11	223	40	1.23	8.62	26.66	15.40	4.41	20.26	5.11	0.89	2.30	0.64	4.90	1.22	4.07	3.45	0.57
CTD8-B12	223	64	1.23	6.33													
CTD8-B13	97	49	1.10	6.68													
CTD8-B14	57	160	3.17	13.34													
CTD8-B15	57	458															

Table 2
Dissolved REE concentrations and Nd isotope data for Niger Delta seawater samples.

Sample	Depth	La	Ce	Pr	Nd	Sm	Eu	Gd	Tb	Dy	Ho	Er	Yb	Lu	Depth	Nd	ε_{Nd}	2 s
	(m)	(pmol/kg)													average			
ER-CTDR-03 — Reference Area																		
CTD3-B1	1776	36.03	34.09	7.12	27.85	5.36	1.21	7.30	1.10	7.58	1.92	6.44	5.22	0.87				
CTD3-B2	1762	27.93	12.57	5.02	20.42	4.06	0.93	5.63	0.88	6.57	1.78	5.69	4.99	0.79				
CTD3-B3	1747	24.85	8.25	4.72	19.16	3.91	0.92	5.31	0.90	6.07	1.70	5.83	5.16	0.89	1710	21.8	−12.5	0.2
CTD3-B4	1682	28.34	10.91	5.04	21.83	3.79	0.93	5.84	0.96	6.59	1.81	5.97	4.98	0.87				
CTD3-B5	1584	27.56	8.79	4.97	19.61	4.09	1.14	5.08	0.88	5.91	1.72	5.57	4.94	0.81				
CTD3-B7	1385	28.72	9.84	5.07	20.35	3.82	1.35	5.84	0.84	6.30	1.70	5.64	5.08	0.82				
CTD3-B8	1187	23.53	5.55	4.40	17.63	3.33	1.03	4.46	0.73	5.18	1.53	4.79	4.90	0.83	1087	17.4	−13.3	0.3
CTD3-B9	987	27.75	4.59	4.31	17.20	3.26	0.99	4.06	0.74	5.34	1.56	5.44	4.97	0.79				
CTD3-B10	788	21.92	4.54	4.48	18.55	3.76	0.91	4.37	0.69	5.04	1.52	5.11	4.56	0.77				
CTD3-B11	588	25.30	5.76	4.78	19.73	3.74	1.12	4.43	0.71	4.94	1.34	4.44	3.73	0.65	487	19.6	−12.4	0.3
CTD3-B12	385	25.11	8.39	4.59	19.51	3.74	1.12	4.56	0.70	4.71	1.24	4.02	2.97	0.51				
CTD3-B13	181	15.84	13.34	3.20	13.77	2.85	0.69	3.51	0.55	3.94	1.09	3.31	2.62	0.38	113	13.7	−15.7	0.5
CTD3-B14	58	17.92	16.65	3.29	13.65	2.65	0.80	3.71	0.54	3.95	1.08	3.25	2.49	0.39				
ER-CTDR-06 — Mud Volcano																		
CTD6-B1	679	28.64	17.38	5.31	21.38	4.04	0.70	5.29	0.78	5.33	1.38	4.68	4.37	0.72				
CTD6-B2	679																	
CTD6-B3	673																	
CTD6-B4	673																	
CTD6-B5	668	29.53	10.91	5.13	20.81	3.91	1.13	5.20	0.80	5.40	1.40	4.70	4.36	0.69	656	21.4	−12.3	0.4
CTD6-B6	658	30.98	11.12	5.37	21.92	3.96	1.24	5.42	0.80	5.60	1.43	4.64	4.04	0.68				
CTD6-B7	618	31.88	11.14	5.33	21.67	3.90	1.17	5.34	0.80	5.40	1.51	4.66	4.15	0.69				
CTD6-B8	618																	
CTD6-B9	553	34.76	16.10	5.68	22.38	3.66	0.40	6.07	0.88	5.78	1.49	4.76	3.91	0.70				
CTD6-B10	498	31.17	11.85	5.60	22.16	4.49	0.79	5.51	0.80	5.45	1.42	4.56	4.11	0.70				
CTD6-B11	458	26.56	8.68	4.68	19.45	3.79	0.72	4.75	0.72	4.89	1.31	4.42	4.02	0.68	435	21.5	−10.7	0.6
CTD6-B12	340	28.49	9.72	4.89	19.90	3.64	1.01	4.99	0.75	5.01	1.33	4.22	3.74	0.60				
CTD6-B14	141	24.82	11.01	4.77	19.96	3.57	1.10	4.81	0.71	4.87	1.25	3.92	3.03	0.49				
CTD6-B15	84	22.73	13.36	4.31	18.04	3.72	1.12	4.70	0.71	5.03	1.25	3.98	3.05	0.48	90	19.6	−13.5	0.4
CTD6-B16	38	23.72	18.79	4.56	19.08	3.82	1.18	5.44	0.81	5.69	1.37	4.31	3.37	0.52				
ER-CTDR-08 — Pockmark Field																		
CTD8-B1	535														534	21.2	−12.1	0.6
CTD8-B3	533	28.13	10.55	5.06	21.16	3.81	0.88	5.09	0.77	5.18	1.33	4.43	3.97	0.70				
CTD8-B4	525	28.88	10.37	5.11	21.02	3.98	0.94	5.12	0.78	5.54	1.42	4.54	4.26	0.73				
CTD8-B6	490	30.22	9.60	5.46	22.68	4.20	0.99	5.29	0.81	5.52	1.43	4.74	4.42	0.74				
CTD8-B7	411														411	22.7	−12.9	0.2
CTD8-B8	411	30.86	9.81	5.49	22.70	4.09	1.00	5.11	0.79	5.38	1.39	4.41	4.04	0.66				
CTD8-B9	335	28.14	9.23	4.96	20.79	3.63	0.89	4.70	0.75	5.05	1.31	4.11	3.81	0.63				
CTD8-B10	283	28.48	9.56	5.20	21.33	4.25	0.89	5.19	0.75	5.19	1.34	4.24	3.85	0.61				
CTD8-B11	223	23.03	7.12	4.12	17.91	3.50	0.80	4.45	0.65	4.53	1.19	3.72	3.36	0.56	223	17.9	−13.5	0.2
CTD8-B12	223																	
CTD8-B13-1	97	14.83	7.02	2.75	11.64	2.43	0.52	3.28	0.52	3.78	1.04	3.44	3.02	0.48				
CTD8-B13-2	97	17.13	7.38	2.84	12.12	2.55	0.56	3.13	0.53	3.87	1.09	3.62	3.09	0.49				
CTD8-B13-3	97	16.24	7.77	3.05	12.92	2.61	0.61	3.52	0.55	4.10	1.11	3.61	3.17	0.49				
CTD8-B14	57	19.97	12.58	4.02	17.28	3.42	0.81	4.48	0.71	4.96	1.25	3.85	3.32	0.51				
CTD8-B15	57														57	17.3	−12.6	0.2

The errors reported here correspond to the measurement errors (note that the external reproducibility is 0.2 ε units).

Table 3
Dissolved REE concentrations for pore water samples at active Niger Delta seeps.

Sample	Core depth	La	Ce	Pr	Nd	Sm	Eu	Gd	Tb	Dy	Ho	Er	Yb	Lu
	(cm)	(pmol/kg)												
Mud Volcano														
ER CS 40	0–2	185	563	65.9	266	49.9	9.3	39.1	6.2	38.5	7.9	23.8	19.0	2.6
Pockmarks														
N2-KI-41	0–2.5	485	1439	133	518	95.1	22.0	74.5	10.0	52.6	10.1	26.7	23.9	3.7
N2-KI-41	15–20	382	1117	103	388	68.5	15.5	67.6	9.0	47.3	9.9	28.2	25.4	4.3
N2-KI-20	0–2.5	723	2177	193	746	139	30.7	111.6	15.3	81.5	15.8	40.8	33.3	4.8
N2-KI-20	5–10	472	1386	124	486	90.7	19.9	73.9	10.2	56.7	11.6	32.6	26.5	4.0
N2-KI-20	75–80	326	870	79.2	319	62.5	16.8	68.5	9.9	59.6	13.2	38.0	31.6	4.9

Table 4
REE concentrations of easily leachable sediment fractions and cold seep carbonates.

Sample	Core depth	La	Ce	Pr	Nd	Sm	Eu	Gd	Tb	Dy	Ho	Er	Yb	Lu
	(cm)	(ppm)												
Dilute HNO_3 sediment (<45 μm fraction) leachates														
N1-KSF-01	0–2	71	238	19.4	74	14.4	3.0	12.8	1.9	9.8	1.8	5.1	3.9	0.52
N1-KSF-42	0–2	79	261	22.6	88	17.3	4.0	15.6	2.1	11.2	2.1	5.8	4.5	0.63
ER-CS-38	0–2	113	371	32.8	132	25.9	5.7	21.6	3.0	14.7	2.6	7.1	5.2	0.70
ER-CS-40	0–2	22	80	9.1	41	10.3	2.4	11.0	1.7	9.1	1.8	4.6	3.6	0.49
Authigenic carbonates														
ER-CS-38	500	8.2	21.0	2.17	8.5	1.59	0.35	1.35	0.21	1.08	0.21	0.56	0.45	0.06
ER-CS-40	5	3.3	7.7	0.85	4.1	0.94	0.21	0.72	0.09	0.45	0.08	0.21	0.15	0.02

Table 5
Nd isotope data for core-top sediment fractions and cold seep carbonate samples.

Sample	Core depth	ε_{Nd}	2 s
	(cm)		
Reference Area			
N1-KSF-01			
Uncleaned forams	0–2	−12.54	0.08
Dilute HNO_3 leachate	0–2	−11.9	0.2
Detrital sediment	0–2	−11.79	0.08
N1-KSF-42			
Uncleaned forams	0–2	−12.69	0.08
Dilute HNO_3 leachate	0–2	−11.2	0.5
Detrital sediment	0–2	−11.70	0.08
Mud Volcano			
ER-CS-40			
Dilute HNO_3 leachate	0–2	−11.2	0.2
Detrital sediment	0–2	−11.23	0.10
Authigenic gypsum	0–2	−11.3	0.2
Authigenic carbonate	5	−11.5	0.2
Pockmark Field			
ER-CS-38			
Uncleaned forams	0–2	−12.50	0.12
Dilute HNO_3 leachate	0–2	−11.1	0.2
Detrital sediment	0–2	−11.79	0.07
Authigenic carbonate	500	−12.0	0.3